Journal of Transport System Engineering 6:1 (2019) 54–67

PREDICTING FRICTIONAL LOSSES GENERATED BY PISTON CONNECTING-ROD BIG END JOURNAL BEARING FOR AN INTERNAL COMBUSTION ENGINE

B. Y. B. Chai[1] and W. W. F. Chong[2*]

[1]School of Mechanical Engineering
Faculty of Engineering
Universiti Teknologi Malaysia (UTM)
81310 Skudai, Johor, Malaysia

[2]Automotive Development Centre (ADC)
Faculty of Engineering
Universiti Teknologi Malaysia (UTM)
81310 Skudai, Johor, Malaysia

Article history
Received
14 April 2019
Received in revised form
10 September 2019
Accepted
11 December 2019
Published Online
29 December 2019

*Corresponding author
william@utm.my

GRAPHICAL ABSTRACT

ABSTRACT

The aim of the study is to investigate the tribological behaviour of the connecting-rod big end journal bearing under dynamic loading for a full engine cycle.In this study, a numerical analysis is used for solving the 2-D Reynolds equation based on Reynolds boundary condition. The 2-D Reynolds solution was derived by using a combination of approaches, namely finite difference method, Newton-Raphson method, and Taylor expansion series. Then, the formulated 2-D mathematical model is used to ascertain the tribological behaviour for both rigid and deformable bearing assumptions.For low loading conditions, the simulation results from both rigid and deformation models have only shown minor differences, demonstrating correlation with existing analytical and experimental results. However, once the loading capacity is increased, the simulation results from the deformation model assumption is shown to be much closer to the experimental results obtained from real engine analysis.In short, an elastic journal bearing assumption in simulating such tribological conjunction is believed to be more practical and reliable for real engine practices as compared to a rigid journal bearing assumption.

KEYWORDS

Tribological; Journal bearing; Numerical analysis; Rigid; Deformation;

1.0 INTRODUCTION

Friction has played a significant role in our daily processes. Fundamentally, friction is known as a type of force, acting in the opposite direction, which tends to resist the motion process between two or more objects. Despite the fact that the existence of this resistance not being desirable, a general life would be impossible without friction, where human beings could face difficulties even walking on the streets. On the other hand, friction has also long existed as one of the biggest challenges in the automotive industries in producing energy efficient vehicles. This will lead to increased fuel consumption and also CO2 emissions. Interestingly, Malaysia has recently been reported to produce the most CO2 emissions from passenger cars in South East Asia (Chong et al. 2018). It has been pointed out that reduction of frictional losses for passenger cars are capable of leading to a threefold improvement in the fuel economy of these vehicles (Holmberg et al., 2012).

A further investigation into the friction of a vehicle, where it can be subdivided into several groups, found that one of the vital systems is the engine system of the vehicle. The engine system contributed almost one-third of the friction in the overall friction that existed in a vehicle. In the one-third of friction held by the engine system, approximately 30% of the engine frictional losses are consumed by bearings (Holmberg et al., 2012). Bearings are frequently found in rotating shafts of an automotive vehicle. One of the major contributors to bearing losses in an engine originates from the piston connecting-rod big end journal bearing, which is attached to the crankshaft. The connecting-rod is an essential part of the crank mechanism in an engine, where power is transmitted from the combustion towards the crankshaft.

Furthermore, a journal bearing that is located at the big end of the connecting-rod is commonly used to reduce friction and give support to rotating elements. Journal bearings typically operate in a hydrodynamic regime of lubrication. The role of the big end journal bearing is to sustain transmitted forces through the connecting rod, which is exerted by the combustion pressure and inertial imbalance, as well as transmission of the torque to drive the crank shaft (Rahnejat, 2010). During operation, the frictional behaviour of this journal bearing is affected by the dynamic loading as a result of the piston motion. Hence, it is vital to be able to accurately predict the frictional losses generated by the piston connecting-rod big end journal bearing in order to improve the performance of an internal combustion engine.Therefore, the study aims to investigate the tribological behaviour of the connecting-rod big end journal bearing under dynamic loading for a full engine cycle.

2.0 GOVERNING EQUATIONS

2.1 2-D Reynolds Equation

Reynolds equation reflects tremendous insight into fluid behaviour in bearing lubricant films especially for bearing under hydrodynamic lubrication. The solution of the Reynolds equation enables one to determine the pressure distribution in a bearing with an arbitrary film shape (Khonsari and Booser, 2008) Therefore, once the pressure profile is evaluated, all the other bearing performance parameters, such as the load-carrying capacity, friction force, and flow rate can be easily determined (Khonsari et al, 2008). A 2-D Reynolds equation given below is employed:

$$\frac{\partial}{\partial x}\left(\frac{\rho h^3}{\eta}\cdot\frac{\partial P}{\partial x}\right)+\frac{\partial}{\partial y}\left(\frac{\rho h^3}{\eta}\cdot\frac{\partial P}{\partial y}\right)=12\left\{\frac{\partial}{\partial x}\left[\frac{\rho h(u_1+u_2))}{2}\right]+\frac{\partial}{\partial y}\left[\frac{\rho h(v_1+v_2))}{2}\right]+\frac{\partial(\rho h)}{\partial t}\right\} \quad (2.1)$$

Before deriving the 2-D Reynolds equation, there will be some assumptions that should be considered to further simplify the 2-D Reynolds equation for fitting the scenario of the study. The assumptions are:

- Newtonian fluid
- Squeeze term is negligible
- The lubricant density and viscosity are constant
- The lubricant flow is laminar and incompressible
- Entrainment velocity in the y-direction is negligible
- Curvature effects are negligible. Hence, allowing the use of Cartesian coordinate system.

From the above assumptions for the Reynolds equation, the final simplified version of the 2-D Reynolds equation can be obtained from Equation 2.2:

$$\frac{\partial}{\partial x}\left(\frac{\rho h^3}{\eta}\cdot\frac{\partial P}{\partial x}\right)+\frac{\partial}{\partial y}\left(\frac{\rho h^3}{\eta}\cdot\frac{\partial P}{\partial y}\right)=12\left\{\frac{\partial(\rho h u)}{\partial x}\right\} \tag{2.2}$$

2.2 Non-Dimensionalization

Before utilizing the simplified version of 2-D Reynolds equation from Equation 2.2, a dimensionless form of 2-D Reynolds equation is determined. The dimensionless form of the 2-D Reynolds equation is shown in Equation 2.3 below (with ρ and η of the lubricant set to be consistent at a single condition):

$$\frac{\partial}{\partial \bar{x}}\left[H^3\cdot\frac{\partial \bar{P}}{\partial \bar{x}}\right]+\frac{\partial}{\partial \bar{y}}\left[H^3\cdot\frac{\partial \bar{P}}{\partial \bar{y}}\right]=\psi\cdot\frac{\partial}{\partial \bar{x}}[H\bar{u}] \tag{2.3}$$

2.3 Finite-Difference Method

From the Equation 2.3 above, the three terms in the equation are then separately expanded by applying the finite difference approximations to achieve a solution in terms of nodal vector (i,j) form. This follows the numerical scheme as proposed by Chong and De la Cruz (2014) and Chong et al. (2014).

$$\begin{aligned}\frac{\partial}{\partial \bar{x}}\left[H^3\cdot\frac{\partial \bar{P}}{\partial \bar{x}}\right] &= \frac{1}{2\Delta\bar{x}^2}\left\{\left[H^3_{i+1,j}+H^3_{i,j}\right]\bar{P}_{i+1,j}-\left[H^3_{i+1,j}+2H^3_{i,j}+H^3_{i-1,j}\right]\bar{P}_{i,j}\right.\\ &\quad\left.+\left[H^3_{i,j}+H^3_{i-1,j}\right]\bar{P}_{i-1,j}\right\}\\ &= A_{i,j}\end{aligned} \tag{2.4}$$

$$\begin{aligned}\frac{\partial}{\partial \bar{y}}\left[H^3\cdot\frac{\partial \bar{P}}{\partial \bar{y}}\right] &= \frac{1}{2\Delta\bar{y}^2}\left\{\left[H^3_{i,j+1}+H^3_{i,j}\right]\bar{P}_{i,j+1}-\left[H^3_{i,j+1}+2H^3_{i,j}+H^3_{i,j-1}\right]\bar{P}_{i,j}\right.\\ &\quad\left.+\left[H^3_{i,j}+H^3_{i,j-1}\right]\bar{P}_{i,j-1}\right\}\\ &= B_{i,j}\end{aligned} \tag{2.5}$$

$$\begin{aligned}\frac{\partial}{\partial \bar{x}}[H\bar{u}] &= \frac{H_{i,j}\bar{u}_{i,j}-H_{i-1,j}\bar{u}_{i-1,j}}{\Delta\bar{x}}\\ &= C_{i,j}\end{aligned} \tag{2.6}$$

The modified Newton-Raphson method is then executed to solve for the Equations 2.4, 2.5, and 2.6 above. The residual term, $F_{i,j}$ of the equation is arranged as shown in Equation 2.7 below:

$$F_{i,j} = A_{i,j} + B_{i,j} - \psi \cdot C_{i,j} \tag{2.7}$$

Taylor expansion series will be used to expand the Equation 2.7 above into Equation 2.8 shown below.

$$\bar{F}_{i,j} = F_{i,j} + \frac{\partial F_{i,j}}{\partial \bar{P}_{i+1,j}} \Delta \bar{P}_{i+1,j} + \frac{\partial F_{i,j}}{\partial \bar{P}_{i-1,j}} \Delta \bar{P}_{i-1,j} + \frac{\partial F_{i,j}}{\partial \bar{P}_{i,j}} \Delta \bar{P}_{i,j} + \frac{\partial F_{i,j}}{\partial \bar{P}_{i,j+1}} \Delta \bar{P}_{i,j+1} + \frac{\partial F_{i,j}}{\partial \bar{P}_{i,j-1}} \Delta \bar{P}_{i,j-1} \tag{2.8}$$

In order to obtain an approximated solution, the residual term in the Taylor expansion series shown in Equation 2.8 has to approach zero.

$$\bar{F}_{i,j} \approx 0$$

After substituting the whole Equation 2.8 by taking$\bar{F}_{i,j} \approx 0$, the equation is rearranged in terms of the change in pressure, $\Delta \bar{P}$ at the midpoint node (i,j). Hence, the change in pressure term is shown in Equation 2.9 below.

$$\Delta \bar{P}_{i,j} = \frac{-F_{i,j} - J_1 \Delta \bar{P}_{i+1,j} - J_2 \Delta \bar{P}_{i-1,j} - J_4 \Delta \bar{P}_{i,j+1} - J_5 \Delta \bar{P}_{i,j-1}}{J_3} \tag{2.9}$$

Equation 2.9 has introduced the Jacobian terms of $J_{1,}$ J_2, J_3, J_4 and J_5. These Jacobian terms are mainly the partial differential of the residual term with respect of their nodal location from the finite difference mesh. The Jacobian terms for hydrodynamic and elastohydrodynamic conditions are dissimilar due to the rheology-pressure relationship of the film thickness term.

2.4 Film Thickness Equation

Film thickness for journal bearing is one of the most vital parameters. For journal bearing under hydrodynamic or elastohydrodynamic regime, the shear friction and power losses of the journal bearing are dominated by the lubrication film as compared to the pressure generated. Hence, pressure distribution will be dependent on the fluid film generated by the journal bearing. According to Wang, Keith, Yang and Kumar (2004), the equation of film thickness for hydrodynamic condition will be demonstrated as in Equation 2.10.

$$h_{i,j} = C\left(1 - \varepsilon_x \cos\theta_i - \varepsilon_y \sin\theta_i\right) \tag{2.10}$$

However, once deformation of the journal bearing is considered, Equation 2.10 will no longer be applicable (Wang et al, 2004). A modified version of fluid film equation, where a new term $\delta_{k,l}$ is to be added to the Equation 2.10, is described below:

$$h_{i,j} = C\left(1 - \varepsilon_x \cos\theta_i - \varepsilon_y \sin\theta_i\right) + \delta_{k,l} \tag{2.11}$$

2.5 Loading Components in Journal Bearing

Loads for a typical journal bearing can be divided into x-direction and y-direction loads. It should be noted that positive x-axis is taken to be horizontal and to the left in the bearing analysis. On the other hand, the positive y-axis is taken to be vertical and downward, which is always pointing from the small end to the big end.The load of the journal bearing can be calculated by using the following Equations 2.12 and 2.13.

$$W_x = \int_{-\pi}^{\pi}\int_{0}^{L} P_{i,j} \cdot cos\theta_i \cdot Rd\theta dy \tag{2.12}$$

$$W_y = \int_{-\pi}^{\pi}\int_{0}^{L} P_{i,j} \cdot sin\theta_i \cdot Rd\theta dy \tag{2.13}$$

2.6 Friction force and power loss

Reynolds equation is applied to compute the fluid film profile of a short journal bearing. From the fluid film and contact pressure distribution, it is now possible to calculate and to formulate the friction force in the connecting-rod big end journal bearing. Typically for a lubricated conjunction, frictional force consists of two main parts namely boundary friction, F_b and viscous friction, F_v.The total friction force is shown in Equation 2.14.

$$F_f = F_b + F_v \tag{2.14}$$

However, due to the case that the minimum film thickness generated by the results for hydrodynamic and elastohydrodynamic conditions are always more than two times the surface roughness between the shaft and the bearing. Hence, boundary friction will not be considered in this study. Therefore, the viscous friction component is formulated as follows:

$$F_f = \tau \cdot A = \tau \cdot dxdy \tag{2.15}$$

where,

$$\tau = \frac{2u\eta}{h_{i,j}} \tag{2.16}$$

Finally, the power losses due to friction can be retrieved from 2.17 below.

$$F_P = F_f \cdot 2u \tag{2.17}$$

3.0 ANALYSIS

3.1 Analytical analysis

In any analysis for journal bearing, the bearing geometry is one of the most important factors that greatly influence the final results for the oil film profile of the journal bearing. Other than that, another important factor is the kinematics properties of the journal bearing during the operation. Table 1 shows the parameters of the journal bearing whereas Figures 1 and 2 have depicted the kinematics properties during the operation.

Table 1 Parameters of journal bearing for verification

Parameters	Values
Bearing radius, R	27.0 mm
Bearing width, L	21.6 mm
Radial clearance, C	27.0 μm
Lubricant viscosity, η	6.89 mPa.s

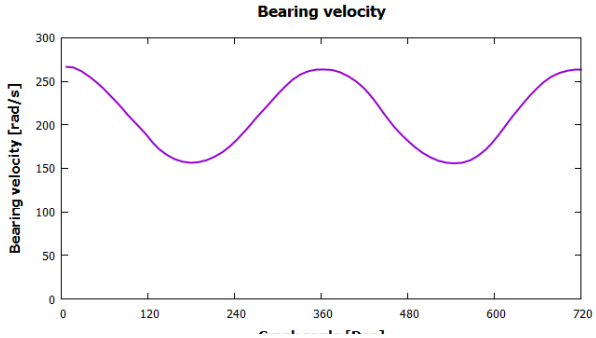

Figure 1 Bearing velocity for a full crank cycle

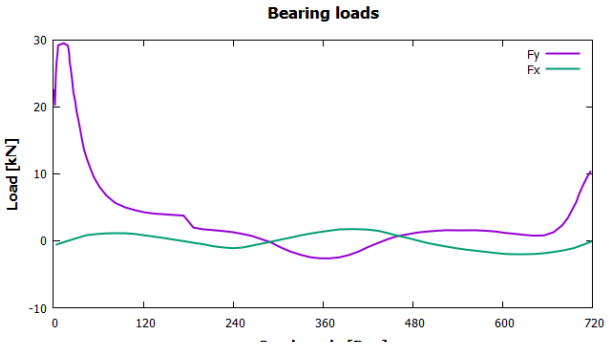

Figure 2 Bearing loads in x and y direction for a full crank cycle

According to Oh and Goenka (1985), Figure 2 shows the loading on the connecting-rod, which includes the gas pressure and the inertia loadings on a six cylinders' gasoline engine. Moreover, Chu (2017) has also conducted a journal bearing analysis based on the exact same paper by using an analytical solution under the Half Sommerfeld boundary condition. In his study, Chu selected four distinct cases for validation purposes. The selected cases are namely:1) Case A (during highest bearing velocity); 2) Case B(during the average bearing velocity); 3) Case C(during lowest bearing velocity) and 4) Case D(during the highest loading in the y-direction, Fy).

3.2 Experimental measurements

An experimental investigation of determining the measurements for minimum oil film thickness in connecting-rod bearings was conductedby Paranjpe et al. (2000). The experimental measurement was carried out by using the Total Capacitance Method (TCM). This method utilizes the bearing as a cylindrical capacitor where the oil in between the bearing and the crankshaft journal is the dielectric medium. All the tests were conducted with a V6 engine running at a steady-state speed of 1500 rpm. The maximum torque (wide open throttle) at this speed was 256 Nm. Figure 3 shows the grasshopper linkage that was used to guide the signal and thermocouple wires in order to avoid bending and failure of wires due to the reciprocating motion of the connecting-rod when experiment is conducted in the testing rig (Paranjpe et al., 2000).

Figure 3 Grasshopper linkage mounted on the connecting-rod(Paranjpe et al., 2000)

The parameters and kinematic properties of the journal bearing to run the whole experiment are shown in Table2 and Figure 4 respectively. The bearing loads are based on 75% of the maximum torque which is only 192 Nm.

Table 2 Bearing parameters for experimental measurements

Parameters	Values
Bearing radius, R	28.6 mm
Bearing width, L	18.1 mm
Radial clearance, C	17.78 µm
Lubricant viscosity, η (5W30 at 100°C)	6.79 mPa.s

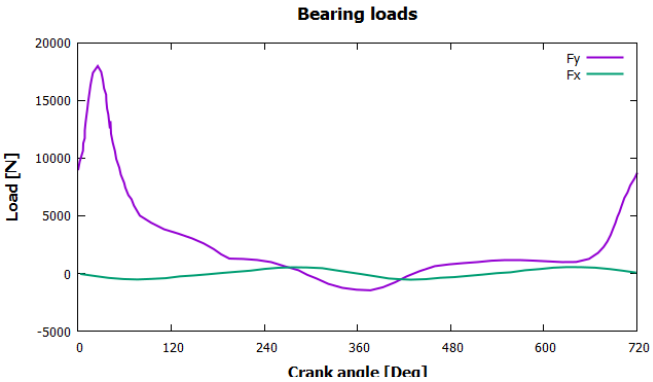

Figure 4 Connecting-rod bearing loads at 1500 rpm

To validate the mathematical model in this study with the experimental measurements, four distinct cases are also selected. The selected cases are specifically at the crank angles:

360°, 458°, 720° and finally 25°, which is right after the Top Dead Center (TDC) of the compression cycle.

4.0 RESULTS AND DISCUSSION

4.1 Validation of Mathematical Model with Analytical solution for Rigid Bearing

All the parameters and kinematics for the simulated journal bearing are obtained from section 3.1. Moreover,Table3 summarize the generated results by using the proposed mathematical model assuming rigid bearing. Such assumption is made in order to have consistency when comparing the current simulation results with reference from Chu (2017).

Table 3 Maximum film pressure, minimum oil film thickness and power loss for the selected cases using the proposed mathematical model for rigid bearing

Case	Maximum Film Pressure (MPa)	Minimum Oil Film Thickness (μm)	Power Loss (W)
A	11.001	4.788	89.496
B	2.995	7.694	45.811
C	16.035	3.119	37.544
D	204.637	1.102	182.340

However, there are some inevitable errors in between the results generated from the proposed mathematical model and the results from the analytical solution. The errors of maximum film pressure, minimum film thickness, and power losses between the analytical solution (Half Sommerfeld boundary condition) and numerical solution (Reynolds boundary condition) are tabulated in Table 4 below.

Table 4 Errors of the results generated between the analytical solution and the proposed mathematical model for rigid bearing

Case	Error in Maximum Film Pressure (%)	Error in Minimum Film Thickness (%)	Error in Power Losses (%)
A	12.52	6.26	0.72
B	10.06	12.49	1.39
C	13.86	1.14	3.68
D	13.42	22.94	15.08

From the results shown in Table 4, it can be noticed that the maximum film pressure, minimum film thickness, and power losses for case A, B and C have errors less than 20%. This shows that the numerical results for these three cases are reasonably similar to the analytical results. However, for case D on the other hand, the error in minimum film thickness for this case has been shown to be higher than the other cases. This shows the unreliability of the mathematical model when it comes to higher loadings condition. In addition, the power losses for case D is significantly higher than the other three cases.

4.2 Validation of Mathematical Model with Analytical solution for Elastic Bearing

Table 5 shows the generated results by using the proposed mathematical model withelastic bearing assumption. The main purpose is to witness the differences of tribological performancein between the rigid and elastic journal bearing. In addition, the study is also to ensure that the proposed mathematical model is adequately robust to distinguish between deformation case from no-deformation case. Nonetheless, the errors in between the results generated from the proposed mathematical model considering deformation and the analytical results from Chu (2017) are shown in Table 6.

Table 5 Maximum film pressure, minimum oil film thickness and power loss for the selected cases using the proposed mathematical model for elastic bearing

Case	Maximum Film Pressure (MPa)	Minimum Oil Film Thickness (μm)	Power Loss (W)
A	10.483	4.670	88.615
B	2.965	7.663	45.635
C	14.469	2.933	37.126
D	77.387	1.317	140.207

Table 6 Errors of the results generated between the analytical solution and the proposed mathematical model for elastic bearing

Case	Error in Maximum Film Pressure (%)	Error in Minimum Film Thickness (%)	Error in Power Losses (%)
A	16.64	3.64	0.46
B	10.96	12.03	0.64
C	22.27	7.04	2.52
D	67.29	7.90	11.51

By comparing Table 4 and Table 6, it can be seen that the deformation model does not affect the lower loading conditions cases. All the errors for cases A, B and C remained as low for both the rigid model and deformation model. However, case D has shown some exceptionally high errors as shown in the results. For instance, the error for maximum pressure has increased significantly from 13.42% to 67.29%. This is due to the huge amount of pressure drop from the deformation model. Once deformation of bearing has been introduced, the maximum film pressure of case D has dropped from 204.637 MPa to 77.387 MPa and has given a slight increase in the minimum oil film thickness from 1.102 μm to 1.317 μm.

Also, when comparing the power losses generated by the journal bearing for both rigid and deformation cases, it can be seen that the deformation model does not show any significant changes onto the power losses in cases A, B, and C when compared with the rigid model. It is noticeable that there is a reduction in the power loss produced by the elastic journal bearing when compared with the power loss generated by the rigid bearing in case D (140.207 W and 182.340 W, respectively). It is evident that when a higher load is exerted onto the journal bearing, high frictional force is produced, resulting in a high power loss when rigid bearing is being considered. Once it is replaced by using an elastic journal bearing, the load will be distributed over a wide range and thus, reducing the power losses generated by the journal bearing.

The oil film profile and the pressure distribution profile for both rigid and deformation results are shown in Figures 5 and 6, respectively.

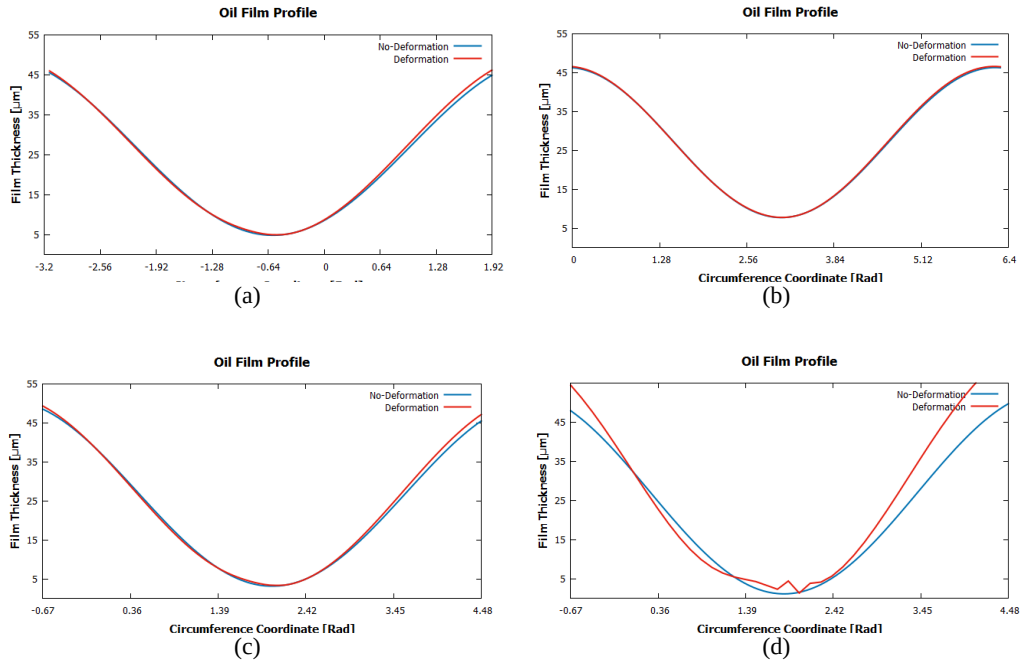

Figure 5 Oil film profile for both rigid and deformation results for (a) Case A, (b) Case B, (c) Case C and (d) Case D

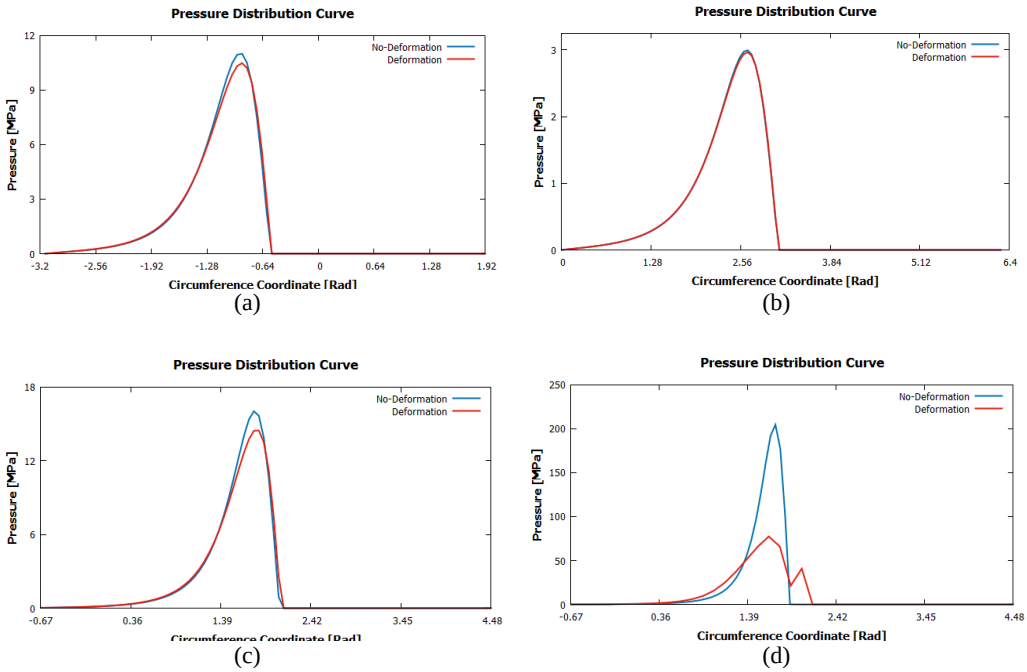

Figure 6 Pressure distribution profile for both rigid and deformation results for (a) Case A, (b) Case B, (c) Case C and (d) Case D

From figures 5 and 6, both the rigid and deformation models have generated quite similar results of the oil film and pressure distribution profiles for case A, B, and C. The only noticeable differences that can be observed are the maximum pressure drop and

minimum oil film thickness increase for the deformed model. In addition, a slight shift of the profile can also be noticed when deformation of bearing is considered. On the other hand, it is noticed that the profiles in case D has shown significant differences when deformation model is applied. Specifically, there is a double peak pressure case existed in case D. When elastic journal bearing is subjected to extremely high loading conditions, the phenomenon of double peak pressure case could exist. According to Wang et al (2004), this particular pressure profile occurs when the oil film thickness varies in the gap between the deformed bearing and the shaft. The gap tends to converge at first, then appears to slightly diverge. After that, it converges again and finally diverges.For instance, there will be a fluctuate of the oil film thickness profile near the minimum point which is depicted in Figure 5(d). Hence, the results from case D will be compared figure-to-figure by referring to the original paper presented by Oh et al. (1985). The oil film profiles are shown in Figure 7 whereas the pressure distribution profiles are shown in Figures 8.

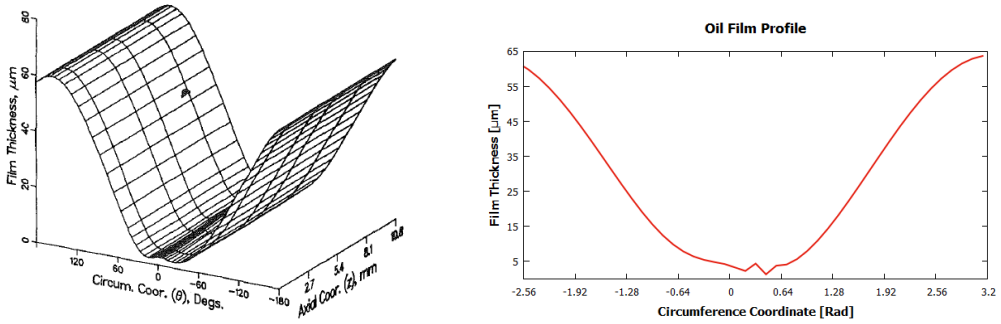

(a) (b)

Figure 7 Oil film profiles for case D from (a) Study done by Oh et al (1985), and (b) Simulation result from deformation model

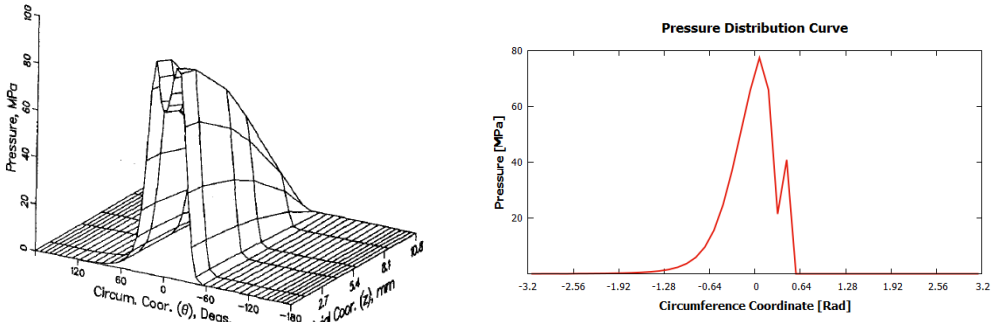

(a) (b)

Figure 8 Pressure distribution profiles for case D from (a) Study done by Oh et al (1985), and (b) Simulation result from deformation model

From figures 8, it can be seen that the maximum pressures between the simulation result and the literature data are closer than the results from the rigid model. The maximum pressure from Figure 8 (a) is approximately 82 MPa whereas the maximum pressure shown in Figure 8 (b) is 77.387 MPa. Also, it is apparent that both the pressure distribution profiles have double peak pressures. Still, the double peak shown in Figure 8 (b) is slightly off as compared to the pressure distribution profile obtained from the paper. This is mainly due to the grid size issue, where finer grid size could yield closer result, requiring longer computational time.

4.3 Validation of Mathematical Model with Experimental measurementsfor Elastic Bearing

Earlier, it was shown that elastic behavior of journal bearing is more reliable when compared with rigid bearing. However, for elastic bearing only the deformation model will be used to validate with the experimental results obtained from real engine analysis. Hence, the simulated results of the minimum oil film thickness for deformation model are tabulated in Table 7 below.

Table 7 Minimum oil film thickness and error with experimental results

Crank Angle	Minimum oil film thickness (µm)	Error of minimum oil film thickness with experimental results (%)
25°	1.956	11.20
360°	4.844	0.44
458°	6.582	9.43
650°	4.692	6.15

From Table 7, it shows that all the results of minimum film thickness for the selected crank angles have small errors when compared to the experimental results. Figure 9 displays the location for these selected cases in a minimum oil film thickness versus full crank angle graph which was retrieved from the experiment.

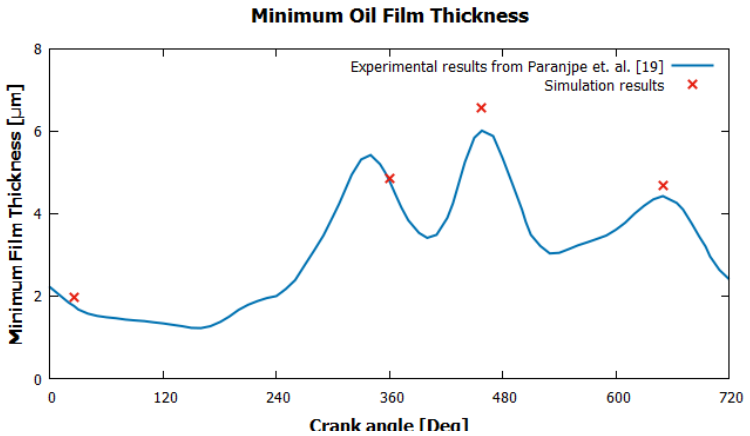

Figure 9 Minimum oil film thickness between simulation results and experimental results

Figure 9shows that the minimum oil film thickness for the simulated results and the literature data are quite close to each other. The simulation results have also shown to have three peaks, which is on the similar trend as the results obtained from the experiment. Other important results, such as the maximum film pressure, friction force and power losses are tabulated down in Table 8.

Table 8 Maximum film pressure, friction force and power losses for the simulation results

Crank Angle	Maximum Film Pressure (MPa)	Friction Force (N)	Power Losses (W)
25°	89.133	17.534	78.773
360°	4.504	8.211	36.888

458°	2.197	7.395	33.221
650°	4.552	8.743	39.276

5.0 CONCLUSION

The reason that numerical approach is being proposed in this study is mainly due to the fact that the analytical approach for Reynolds boundary condition does not consider for deformation. The results generated by the numerical approach is as close as the analytical approach when it comes to lower loading conditions on the journal bearing. Once a higher loading condition is subjected onto the journal bearing, elastic deformation will occur and the results from numerical approach will significantly vary from the analytical approach. This study has evidently proven that when it comes to a higher loading condition in the journal bearing, specifically at the power stroke of an engine, an elastic journal bearing is more suitable as compared to a rigid bearing. On the other hand, the study of the pressure and oil film behaviour of journal bearing has allowed us to measure the power losses generated due to friction from the journal bearing. In short, power loss directly examines the efficiency of a vehicle. Overall, elastic journal bearing has been shown to be more practical than rigid bearing in real life practice. It reduces the pressure exerted onto the journal bearing and thus, decreases the power loss generated due to friction from the journal bearing.

REFERENCES

[1] Chong, W.W.F., Ng, J.-H., Rajoo, S., & Chong, C.T. (2018). Passenger transportation sector gasoline consumption due to friction in Southeast Asian countries. Energy conversion and management, 158, 346-358.

[2] Chong, W.W.F., & De la Cruz, M. (2014). Elastoplastic contact of rough surfaces: a line contact model for boundary regime of lubrication. Meccanica, 49(5), 1177-1191.

[3] Chong, W.W.F., Teodorescu, M., &Rahnejat, H. (2014). Mixed thermo-elastohydrodynamic cam–tappet power loss in low-speed emission cycles. International Journal of Engine Research, 15(2), 153-164.

[4] Chu, J.H. (2017).A Friction Study on Automotive Connecting-Rod Big End Journal Bearing Lubrication System. UGP Thesis,UniversitiTeknologi Malaysia, Skudai.

[5] Holmberg, K., Andersson, P., &Erdemir, A. (2012). Global energy consumption due to friction in passenger cars. Tribology International, 47, 221-234.

[6] Khonsari, M.M. and Booser E.R. (2008).Applied Tribology – Bearing Design and Lubrication, 2nd Edition. John Wiley & Sons, Ltd Publishing.

[7] Oh, K. P., &Goenka, P. K. (1985). The elastohydrodynamic solution of journal bearings under dynamic loading. *Journal of Tribology*, *107*(3), 389-394.

[8] Paranjpe, R. S., Tseregounis, S. I., & Viola, M. B. (2000). Comparison between theoretical calculations and oil film thickness measurements using the total capacitance method for crankshaft bearings in a firing engine. *Tribology transactions*, *43*(3), 345-356.

[9] Rahnejat, H. (2010). Tribology and dynamics of engine and power train.Woodhead Publishing Limited.

[10] Wang, D., Keith, T. G., Yang, Q., & Kumar, V. (2004). Lubrication analysis of a connecting-rod bearing in a high-speed engine. Part I: rod and bearing deformation. *Tribology transactions*, *47*(2), 280-289.